Polymorphism in 2-X-Adamantane Derivatives (X = Cl, Br)

Philippe Négrier, María Barrio, Josep Ll Tamarit, Denise Mondieig

Polymorphism in 2-X-Adamantane Derivatives (X = Cl, Br)

Philippe Negrier,[†,‡] María Barrio,[§] Josep Ll. Tamarit,[*,§] and Denise Mondieig[†,‡]

[†]Univ. Bordeaux and [‡]CNRS, LOMA, UMR 5798, F 33400 Talence, France

[§]Grup de Caracterització de Materials, Department de Física i Enginyeria Nuclear, Universitat Politècnica de Catalunya, ETSEIB, Diagonal 647, 08028 Barcelona, Catalonia, Spain

ABSTRACT: The polymorphism of two 2 X adamantane derivatives, X = Cl, X = Br, has been studied by X ray powder diffraction and normal and high pressure (up to 300 MPa) differential scanning calorimetry. 2 Br adamantane displays a low temperature orthorhombic phase (space group $P2_12_12_1$, Z = 4) and a high temperature plastic phase ($Fm3m$, Z = 4) from 277.9 ± 1.0 K to the melting point at 413.4 ± 1.0 K. 2 Cl adamantane presents a richer polymorphic behavior through the temperature range studied. At low temperature it displays a triclinic phase ($P1$, Z = 2), which transforms to a monoclinic phase ($C2/c$, Z = 8) at 224.4 ± 1.0 K, both phases being ordered. Two high temperature orientationally disordered are found for this compound, one hexagonal ($P6_3/mcm$, Z = 6)a t ca. 241 K and the highest one, cubic ($Fm3m$, Z = 4), being stable from 244 ± 1.0 K up to the melting point at 467.5 ± 1.0 K. No additional phase appears due to the increase in pressure within the studied range. The intermolecular interactions are found to be weak, especially for the 2 Br adamantane compound for which the Br···Br as well as C−Br···H distances are larger than the addition of the van der Waals radii, thus confirming the availability of this compound for building up diamondoid blocks.

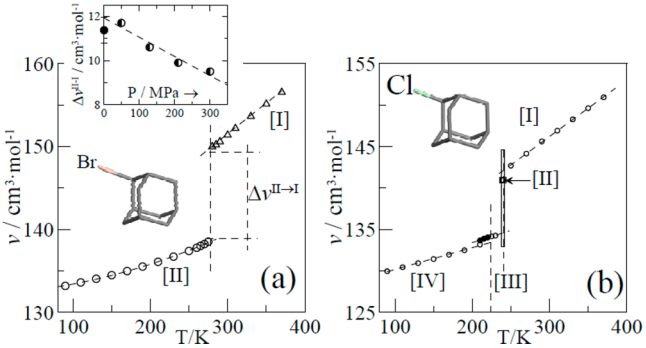

1. INTRODUCTION

Within the field of solid state of organic molecular compounds, one of the most recent challenges concerns the understanding of functional groups that form weak solid state interactions because they have been proved to be of great interest for building up organic crystals with large cavities with useful physical and chemical properties.[1−5] Applications spread for a great variety of fields as nanotechnology, pharmaceutical, chemical processes, or biological domains.[6−12] In these fields, the number of molecular building blocks, which can be used in the exponentially developed crystal design world, is continu ously increasing. Among these new materials, diamondoid systems, a set of hydrocarbons fully sp^3 hybridized formed by three or more interwoven cyclohexane rings, have recently received a great interest. The most simple diamondoid element corresponds to the adamantane molecule. The adamantane molecule ($C_{10}H_{16}$) is formed by a 10 carbon cage made of four cyclohexane rings in chair conformation. Adamantane, a well known compound displaying a wide temperature range of the plastic phase (from 208 to 543 K)[13] due to the molecular spherical shape (T_d symmetry), can react via the carbon sites, four being three coordinated (tertiary) whereas six of them are two coordinated (secondary). The plastic phases (also called orientationally disordered (OD) phases) are intermediate phases between the liquid and the completely ordered low temperature crystalline phase in which the molecules perform reorientations more or less freely among a set of distinguishable number of equilibrium orientations that after a time average generally yield a high space group symmetry lattice (hexagonal or cubic). For adamantane, the plastic phase has carefully been characterized by means of many dynamical as well as structural studies, which demonstrate that molecular reorientations are accompanied by uniaxial rotations, giving rise to a $Fm3m$ space group.[13−22] The tertiary carbon atoms of adamantane are highly reactive, so a large number of 1 X adamantane derivatives (X = F, Cl, Br, I, OH, COOH, etc.) can be easily obtained. These 1 X adamantane derivatives displaying a C_{3v} ($3m$) point group symmetry show a rich polymorphic behavior that has largely been characterized.[23−31] The secondary carbon atoms are much less reactive, and thus substitution to obtain 2 X adamantane derivatives (with C_{2v}, $mm2$, molecular symme try) is performed through the previous production of 2 adamantone (X = O) by substituting two methylene hydrogen atoms attached to a secondary carbon. While these 2 X adamantane systems have not yet been studied to the extent that the 1 X adamantane systems have been, some early explorations have been found in the literature. They mainly concern the X = O[21,31−40] and X = OH[41−43] derivatives. The lack of structural data for the 2 X adamantane compounds, with the exception of 2 adamantanone,[21,33,37] is probably due to the particular difficulty and complexity in growing single crystals at low temperature.

The experimental substances dealt with in this paper are two 2 X adamantane derivatives, 2 Cl adamantane ($C_{10}H_{15}Cl$) and 2 Br adamantane ($C_{10}H_{15}Br$), referred to as 2 Cl A and 2 Br A, respectively, hereinafter. The purpose of this work is to describe the polymorphic behavior of both compounds at normal and high pressure. The structures for all involved phases have been determined for the first time and are compared between them. The rationale behind this polymorphic study is to test whether the intrinsic weak intermolecular interactions within adaman tane based diamondoid structures are already present in the materials in which they are originated.

2. EXPERIMENTAL SECTION

2.1. Materials. 2 Br A was purchased from Aldrich, while 2 Cl A was obtained from ABCR, both with purity better than 98%. Compounds were submitted to a process of slow sublimation at temperatures within the range of the OD phase. The purification process was checked by differential thermal analysis through the change of the melting temperature as well as the peak shape. Figure 1 details, for 2 Br A, the strong influence of the purity of the sample on the melting transition.

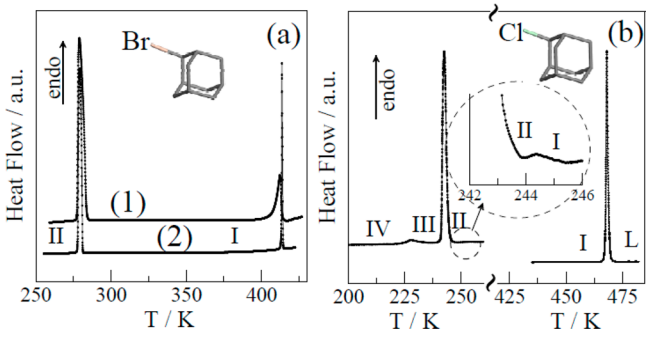

Figure 1. (a) DTA curves for 2 Br A for the as received (1) and purified (2) samples. (b) DSC curves for 2 Cl Ad. Inset describes a ca. 100 times magnification of the II−I transition.

2.2. Differential Thermal Analysis at Normal Pressure. Thermal properties of the phase transitions (temperatures and enthalpy changes) of 2 Br A and 2 Cl A were determined by means of two TA Instruments analyzers: The Q100 analyzer, equipped with an intracooler system, was used for temperatures higher than 200 K, while a TA2920 system equipped with a LCNA liquid nitrogen cooling device was used for measure ments at lower temperatures. Heating and cooling rates of 2 K min^{-1} under a constant nitrogen stream of 25 mL min^{-1} and sample masses of ∼10 mg were used.

2.3. High-Pressure Differential Thermal Analysis. High pressure differential thermal analysis measurements were carried out at a 2K min^{-1} heating rate by means of an in house built high pressure differential thermal analyzer similar to Würflinger's apparatus.[44,45] Temperature and pressure ranges were between 200 and 470 K and 0 and 300 MPa. Both 2 Br A and 2 Cl A were mixed with inert perfluorinated liquid (Galden, Bioblock Scientifics, France) before the high pressure pans were closed to make sure that in pan volumes were free of air. To verify that the perfluorinated liquid was chemically inactive when mixed with both compounds and thus that it would not affect their transition temperatures, we performed normal pressure DTA runs of mixtures using TA Q100 instrument.

2.4. X-ray Powder Diffraction Measurements. X ray powder diffraction data were collected by means of a horizontally mounted INEL cylindrical position sensitive detector (CPS120). The detector, used in Debye−Scherrer geometry, consisted of 4096 channels, providing angular step of 0.029°(2θ) between 4 and 120°. Monochromatic Cu $K_{\alpha 1}$ radiation (λ = 1.5406 Å) was selected with asymmetric focusing incident beam curved quartz monochromator. The angular linearity deviation in PSD (position sensitive detector) was corrected according to the recommended procedure, external calibration using the $Na_2Ca_2Al_2F_{14}$ cubic phase mixed with Silver Behenate, and was performed by means of cubic spline fittings.[46] The generator power was set to 1.0 kW (40 kV and 25 mA). The peak positions were determined by pseudo Voigt fittings using the Peakoc application from Diffractinel software.[47] Samples were introduced into 0.3 mm diameter Lindemann capillaries by melting. Capillaries rotate along their longitudinal axes during data collection, both features trying to prevent effects of preferred orientations.

Diffraction patterns as a function of temperature in the range 90−370 K were carried out by using a liquid nitrogen 600 series Cryostream Cooler device from Oxford Cryosystems with temperature accuracy of 0.1 K. X ray profiles were acquired isothermically upon cooling first then heating back so that the temperature range was scanned at intervals of ca. 20 K and less when a transition was approached. Acquisition times were at least 60 min, and a stabilization time of at least 5 min at each temperature before data acquisition was selected. Longer time acquisition patterns were obtained at different temper atures for structural and refinement purposes.

Indexing of the X ray powder diffraction patterns, structure solutions, and Pawley and Rietveld refinements were performed using Materials Studio Program (MS Modeling (Materials Studio), version 5.5: http://www.accelrys.com).[48]

3. RESULTS

3.1. Thermodynamic Results. Temperature and enthalpy changes at the solid−solid and melting transitions determined by means of DTA (see Figure 1) at normal pressure are summarized in Table 1, together with some values previously reported, to which they match up within the experimental error. As for 2 Br A, it is worth noticing that purification process strongly modifies the thermodynamic properties of the melting, whereas for the II−I transition the influence is almost negligible. Similar results were found for 2 Cl A, although transition temperatures are slightly modified under the sublimation process. We should emphasize the rich poly morphic behavior of 2 Cl A, with four solid phases. It should be highlighted that transition II−I at ca. 244.0 K was never reported, probably due to the small enthalpy change and its closeness with the III−II transition.

High pressure DTA experiments were conducted to determine the II−I and melting transitions for 2 Br A. As for 2 Cl A, only III−II transition (probably with the II−I transition involved) was determined due to the small enthalpy change of the IV−III and II−I solid−solid transitions. As for the melting of 2 Cl A, the temperature domain was beyond the available temperature range of the experimental device. Figure 2 displays the determined pressure−temperature ($p-T$) two phase equilibria for both compounds.

3.2. Structure Determination of Phase II of 2-Br-A. The lattice of the low temperature phase II was determined as orthorhombic at 260 K by means of X Cell software, available

Table 1. Transition Temperatures (T_c) and Enthalpy (ΔH) and Entropy Changes (ΔS) Derived from DTA Measurements and Volume Changes Determined from X ray Powder Diffraction Measurements (Δv^{XR}) and from the Slope of the Pressure−Temperature Two Phase Equilibria $(dT_c/dp)^{exp}$ Derived from the Application of the Clausius−Clapeyron Equation $(dT_c/dp)^{CC}$ at Normal Pressure (Δv^{HP}) for 2 Br Adamantane ($C_{10}H_{15}Br$) and 2 Cl Adamantane ($C_{10}H_{15}Cl$)

$C_{10}H_{15}Br$		
property	II ($P2_12_12_1$)→ I(FCC)	I(FCC) → L
T_c/K	277.9 ± 1.0	413.4 ± 1.0
ΔH/kJ mol^{-1}	12.09 ± 0.33	3.21 ± 0.24
ΔS/J mol^{-1} K^{-1}	43.5 ± 1.2	7.76 ± 0.57
Δv^{XR} (p = 0.1 MPa)/cm^3 mol^{-1}	11.37 ± 0.57	
Δv^{HP}(*) (p = 0.1 MPa)/cm^3 mol^{-1}	10.56 ± 0.60	0.466 ± 0.093
$(dT_c/dp)^{exp}$ K MPa^{-1}	0.243 ± 0.006, (0.235 ± 0.011)[a]	0.601 ± 0.073

$C_{10}H_{15}Cl$				
property	IV($P\bar{1}$) → III($C2/c$)	III($C2/c$) → II(H)	II(H) → I(FCC)	I(FCC) → L
T_c/K	224.4 ± 1.0 227[b]	240.9 ± 1.0 242[b]	244.0 ± 1.0	467.5 ± 1.0
ΔH/kJ mol^{-1}	0.48 ± 0.05 0.47[b]	8.27 ± 0.68 8.31[b]	0.17 ± 0.10	5.30 ± 0.16
ΔS/J mol^{-1} K^{-1}	2.15 ± 0.22 2.3[b]	34.3 ± 0.5 35[b]	0.7 ± 0.5	11.34 ± 0.34
Δv^{XR} (p = 0.1 MPa)/cm^3 mol^{-1}	0.53 ± 0.12	6.35 ± 0.40	1.1 ± 0.4	
Δv^{HP} (p = 0.1 MPa)/cm^3 mol^{-1}		6.80 ± 0.66		
$(dT_c/dp)^{exp}$/K MPa^{-1}		0.198 ± 0.003		

[a]Ref 38. [b]Ref 39.

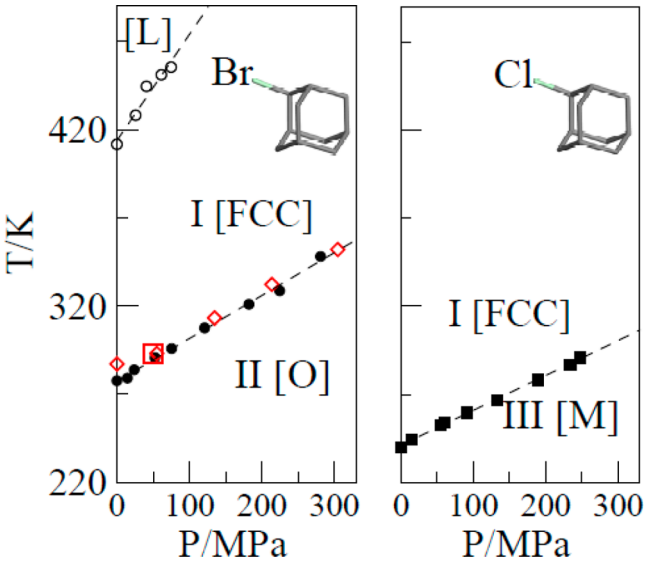

Figure 2. Pressure−temperature phase diagram of (a) 2 Br A, obtained from high pressure DTA (circles) (empty square from ref 40 and diamonds from ref 38) and (b) for the III (monoclinic) to II (hexagonal) to I (FCC) phase transitions of 2 Cl A.

in the module *Powder Indexing of Materials Studio*.[48] Systematic absences enable us to determine the space group, which was compatible with $P2_12_12_1$ space group, and according to a reasonable density and compatibility between volume changes at the II−I transition derived from the Clausius−Clapeyron equation, Z = 4 was assigned. A rigid body molecule was built up by using the cage body obtained for similar adamantane derivatives.[21,25,26,29] Pawley refinement, which minimizes the weighted R factor, R_{wp}, describing the agreement between the experimental pattern and the simulated one, helps to confirm the indexing result and the systematic absences, thus confirming the space group. The unit cell parameters, zero point shift, background, peak profile (pseudo Voigt), and peak asymmetry parameters were also refined. (See Table 2.) For the final Rietveld refinement, the position and orientation of the molecule within the rigid body constraint with a single overall isotropic displacement parameter and preferred orientation by using the Rietveld−Toraya function were refined.[49,50] The final refined pattern is depicted in Figure 3 together with the experimental and refined pattern difference. Table S1 in Supporting Information gathers the fractional coordinates for the orthorhombic structure at 260 K.

3.3. Structure Determination of Phases IV and III of 2-Cl-A. Following similar procedures, the high resolution X ray powder diffraction patterns were used to solve the structures of phases IV and III of 2 Cl A at 100 and 230 K, respectively. After indexing the patterns, systematic absences were found to be compatible with P_1 and $C2/c$ space groups for phases IV and III, respectively. The number of molecules within the unit lattice, Z = 2 for phase IV and Z = 8 for phase III, were assigned according to physically rational density values as well as to make them compatible with volume change values derived from the Clausius−Claperyon equation.

Table 2 compiles the results for the refined parameters of the final Rietveld refinement, while Figure 4 depicts the final refined patterns for both ordered phases IV and III.

3.4. Orientationally Disordered Phases of 2-Br-A and 2-Cl-A. Because of the orientational disorder of phase I of 2 Br A, structural analysis was limited to a Pawley profile fitting according to a face centered cubic lattice symmetry with a lattice parameter of a = 10.0212(7) Å at 300 K. This lattice symmetry agrees with previous single crystal X ray diffraction results from Shimoikeda and Machida.[51] These authors were unable to determine the space group due to the reduced number of Bragg reflections and to the fast dynamics of this OD phase, as inferred from the low activation energy obtained by means of NMR measurements. Owing to the similarities of

Table 2. Results from the Rietveld Refinement of the Low Temperature Ordered Phases of 2 Br A ($C_{10}H_{15}Br$) and 2 Cl A ($C_{10}H_{15}Cl$)

chemical formula	$C_{10}H_{15}Br$	$C_{10}H_{15}Cl$	
M/g mol^{-1}	215.130	170.679	
phase	II	IV	III
2θ-angular range	15 80°	5 65 °	5 65 °
space group	$P2_12_12_1$	$P\bar{1}$	$C2/c$
a/Å	6.5912 ± 0.0007	6.4681 ± 0.0015	25.475 ± 0.005
b/Å	8.2254 ± 0.0009	6.7071 ± 0.0014	6.6142 ± 0.0008
c/Å	16.8717 ± 0.0015	11.012 ± 0.002	11.9851 ± 0.0017
α/deg	90	91.016 ± 0.017	90
β/deg	90	90.85 ± 0.02	118.211 ± 0.014
γ/deg	90	115.238 ± 0.013	90
V/Z/Å^3	228.68 ± 0.04	215.97 ± 0.08	222.43 ± 0.02
Z (Z')	4(1)	2(1)	8(1)
temperature	260 K	100 K	230 K
D_x/g cm^{-3}	1.5622 ± 0.0003	1.3123 ± 0.0005	1.2742 ± 0.0002
radiation type: X-ray, λ	λ=1.5406 Å	λ=1.5406 Å	λ=1.5406 Å
2θ-shift (zero correction)	0.0559 ± 0.0007	0.0024 ± 0.0011	0.0133 ± 0.0007
Profile Parameters			
Na	0.194 ± 0.010	0.377 ± 0.011	0.343 ± 0.007
Reliability Parameters			
R_{wp}	6.07%	6.55%	4.79%
R_p	4.24%	4.66%	3.52%
Peak Width Parameters			
U	0.138 ± 0.014	0.63 ± 0.05	0.360 ± 0.026
V	0.0571 ± 0.008	0.062 ± 0.017	0.052 ± 0.011
W	0.028 ± 0.001	0.020 ± 0.002	0.017 ± 0.001
overall isotropic temperature factor, U/Å^2	0.0514 ± 0.0007	0.038 ± 0.001	0.0776 ± 0.0010
Preferred Orientation (Rietveld Toraya Function)[49,50]			
a*	0.04 ± 0.02	0.485 ± 0.009	0.5040 ± 0.0000
b*	0.269 ± 0.004	0.648 ± 0.011	0.5464 ± 0.0000
c*	0.962 ± 0.001	0.586 ± 0.011	0.6689 ± 0.0001
G2	3.29 ± 0.17	0.24 ± 0.08	0.368 ± 0.026
G1	0.316 ± 0.009	0.00 ± 0.26	0.013 ± 0.044

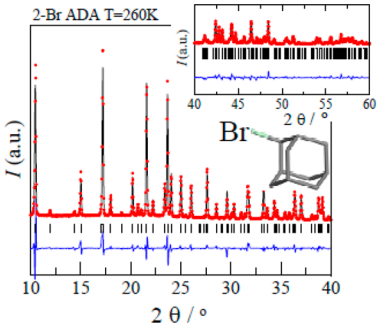

Figure 3. Experimental (red circles) and calculated (black line) diffraction patterns along with the difference profile (blue line) and Bragg reflections (vertical sticks) of orthorhombic $P2_12_12_1$ space group phase II of 2 Br A at 260 K. Inset corresponds to the scale for the data between 40 and 60 2θ°.

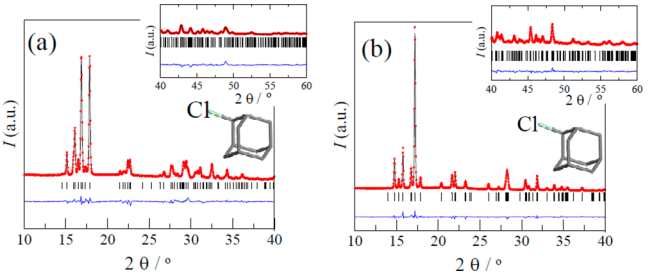

Figure 4. Experimental (red circles) and calculated (black line) diffraction patterns along with the difference profile (blue line) and Bragg reflections (vertical sticks) of the phases (a) IV (triclinic, $P1$) and (b) III (monoclinic, $C2/c$) of 2 Cl A at 100 and 230 K, respectively. Insets correspond to the scale for the data between 40 and 60 (2θ°).

the phase I patterns of 2 Br A and 2 Cl A compounds and that of 1 cyanoadamantane,[28] the $Fm3m$ space group was assigned.

To disentangle the phase behavior of 2 Cl A within the temperature domain where transition from phase III to phase I through phase II takes place, we collected X ray powder diffraction patterns every 2 K around the phase transition from phase III to phase I. Some of these patterns are shown in Figure 5. This Figure shows that patterns of phase II were always obtained together with the low (phase III) or high (phase I) temperature phases. This experimental fact matches up with that found by using differential thermal analysis, which underlines the closeness of the phase transitions (Figure 1b). It should be noticed, in addition, that on cooling from phase I, transition to phase II is bypassed and the sample transforms to phase III with an hysteresis of ca. 10 K.

Despite the fact that a clean pattern of phase II could not be obtained, Pawley refinement was applied to a pattern measured at 240 K, in which phases II and I coexist. The difference of the temperature obtained by X ray diffraction and the DSC

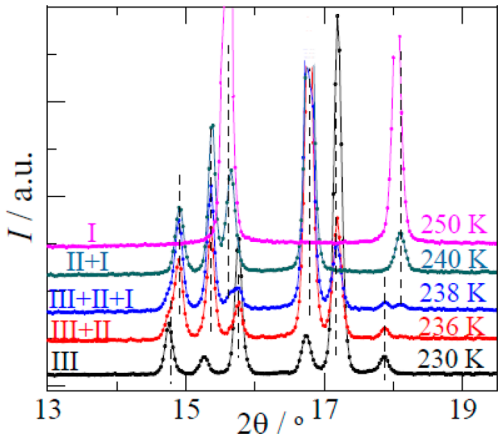

Figure 5. Some X ray powder diffraction patterns collected as a function of temperature around the phase III to phase I temperature domain.

technique can be associated with the dynamical differences between both techniques. The pattern was indexed according to the hexagonal symmetry, and according to the systematic extinctions, even the $P6_3/mcm$ space could be tentatively assigned. Lattice parameters were determined to be a = 11.868(4) Å and c = 11.509(4) Å, V/Z = 233.98 ± 0.02 Å^3, and Z = 6. The goodness of the Pawley refinement is depicted in Figure 6.

As far as the OD phase I of 2 Cl A is concerned, after indexing the pattern according to the face centered cubic lattice symmetry, an academic exercise to determine the structure was envisaged. By assuming the *Fm*3*m* space group, compatible with the systematic extinctions, Rietveld refinement was undertaken with the rigid molecule. Such a procedure gives a molecule place, as described in the inset of Figure 7.

4. DISCUSSION

4.1. Low-Temperature Ordered Phases. The low temperature orthorhombic ordered phase of 2 Br A consists of molecules forming planes stacking perpendicular to ***a*** axis, with the molecular dipole (C1−Br direction) mainly parallel to the *c* axis. Figure 8a corresponds to the (*h*0*l*) crystallographic plane and shows that two adjacent planes perpendicular to the

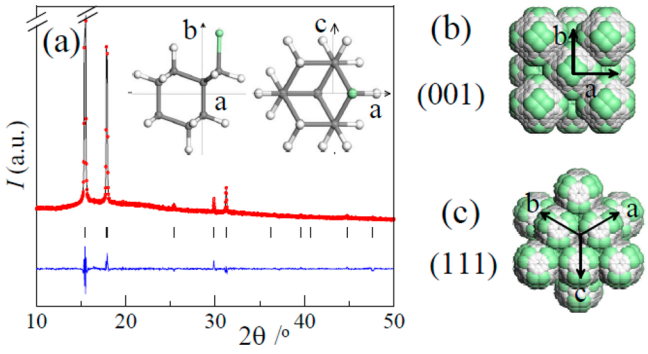

Figure 7. (a) Experimental (red circles) and calculated (black line) diffraction patterns along with the difference profile (blue line) and Bragg reflections (vertical sticks) of face centered cubic *Fm*3*m* space group phase I of 2 Cl A at 310 K. Inset corresponds to the location of the asymmetric unit in the (001) and (010) cubic planes. (b,c) (001) and (111) projections of the unit cell, respectively, according to the *Fm*3*m* space symmetries applied to the Cl adamantane molecule place as described in the inset of panel a.

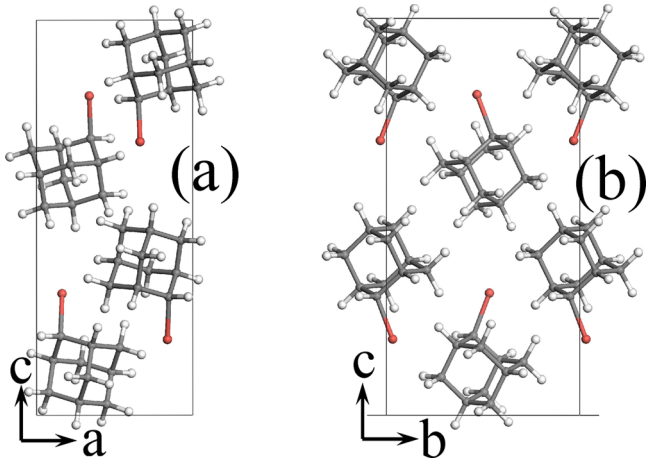

Figure 8. (a) (*h*0*l*) and (b) (0*kl*) crystallographic planes of the low temperature phase II of 2 Br A at 260 K.

a axis have the dipole moments aligned in opposite direction. Figure 8b, the (0*kl*) crystallographic plane, shows that dipoles

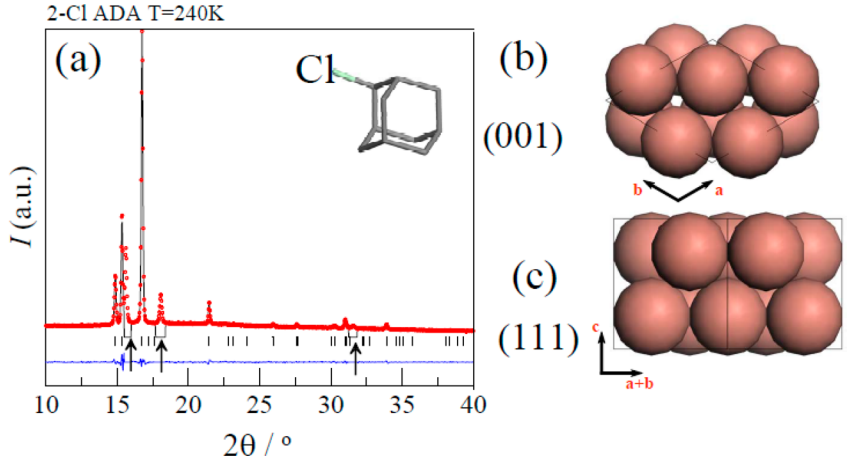

Figure 6. Experimental (red circles) diffraction pattern and calculated (black line) diffraction pattern by Pawley fitting procedure along with the difference profile (blue line) and Bragg reflections (vertical sticks) of hexagonal phase II at 240 K. Excluded regions (see arrows) correspond to phase I (FCC) Bragg reflections. (b,c) (001) and (111) projections of the hexagonal unit cell, respectively.

are slightly tilted 20.6° and they lay almost over the (*h*0*l*) (just 1.9° tilted) planes. The Br···Br distances are really large (the shortest one being 5.035 Å, much longer than the addition of the van der Waals radii) and thus minimize the halogen··· halogen interactions. The shortest C−Br···H distances are 2.974(5) and 3.025(3) Å, which means that there are no distances less than the van der Waals between stacked molecules.

Figure 9 displays the (*h*0*l*) crystallographic plane of the triclinic phase IV and monoclinic phase III of 2 Cl A at 100 and

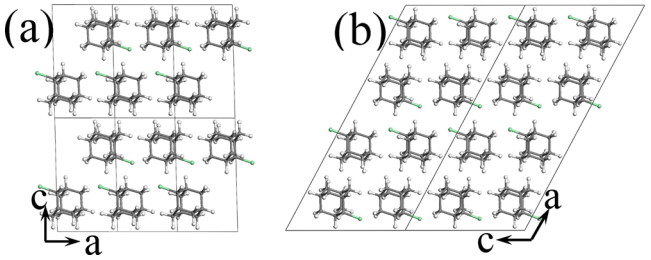

Figure 9. (*h*0*l*) crystallographic planes of the low temperature phase II at 100 K (a) and of the monoclinic phase III at 230 K (b) of 2 Cl A.

230 K, respectively. Despite the low symmetry of phase IV (*P*1 space group), the overall packing is quite similar to that of the monoclinic (*C*2/*c* space group) phase III. Dipoles lay closely to a plane perpendicular to the *b* axis. The intercalated molecular sheets also contain molecules with the molecular dipoles being oppositely oriented in two adjacent layers.

As far as shortest Cl···Cl distances are concerned (see CIF file in the Supporting Information), it can be seen that they are 3.689(5) Å, so Cl atoms in this phase are much closer (not far away from the addition of the van der Waals radii) than Br ones in the orthorhombic phase II of 2 Br A, which means that interactions in phase IV of 2 Cl A are stronger. In the monoclinic phase III, the shortest Cl···Cl increases to 3.830(7) Å. In both triclinic and monoclinic phases of 2 Cl A, C−Cl···H bonds are 2.599(9) and 2.825 Å, respectively and thus are really close (or even less) to the van der Waals radii, confirming the strongest bonds in the low temperature phases of 2 Cl A.

The molecular arrangement maximizing the intermolecular Br···Br distances has also been found in some other much simpler molecular compounds.[52] In fact, the Br···Br interactions have been found to be so weak in tetraphenylmethane derivatives that they can be exchangeable by C−H···C−C weak hydrogen bonds; this fact plays a crucial role when substituents are attached to adamantane core to build up interwoven diamondoid lattices.[53]

Phase transition of 2 Cl A from phase IV to phase III occurs without a big distortion of the overall molecular packing, as demonstrated from the similar packing (see Figure 9) as well as from the small volume change. (See Table 1.) Molecules are rearranged within a higher symmetry lattice (monoclinic, *C*2/*c* space group) but keep the layering structure. (See Figure 9.)

4.2. High-Temperature Orientationally Disordered Phases. The lattice symmetry of the OD phase I of 2 Br A and 2 Cl A has been found to be *Fm*3*m* from the Rietveld refinement procedure. The choice of the space group has been performed on the previous results for other adamantane derivatives, among them, 1 X adamantane, for X = F, Cl, Br, I, and CN, for which some detailed single crystal X ray and neutron scattering experiments have previously been pub lished.[26,28−30] It is worth pointing out that these 1 X adamantane derivatives have a 3m molecular symmetry and thus are compatible with the *Fm*3*m* space group. Nevertheless, for 2 X adamantane, the molecular symmetry (*mm*2) would be incompatible, unless the orientational disorder makes it possible through the molecular tumbling.[21,26] This was proved for 2 adamantanone (X = O), for which despite the *mm*2 molecular symmetry the same space group was settled by means of a cubic harmonic analysis showing that Frenkel model, for which the mean molecule has *n* equilibrium positions each one with 1/*n* Dirac probability, is able to describe the disordered structure.[21] Our Rietveld refinement academic exercise applied to 2 Cl A is based on these grounds.

As for the hexagonal lattice of phase II of 2 Cl A, it can be seen that the lattice parameter c^{H} (11.509 Å) equals ∼2/3 of the (111) diagonal of the cubic lattice ($c^{H} = 2/3*\sqrt{3}*a^{FCC} = 2a^{FCC}/\sqrt{3}$, with a^{FCC} = 9.8228 Å at 250 K), which means that the molecular stacking of the hexagonal (001) crystallographic planes is the same as that of the (111) planes of the cubic phase. This result can be easily seen by comparing Figure 6b with Figure 7c. The corresponding $a^{H} = b^{H}$ hexagonal lattice parameters calculated through the cubic lattice would be $((6/4)^{1/2}*a^{FCC})$ 12.03 Å, really close to the experimental hexagonal parameter (a^{H}=11.87 Å). Needless to say that the so obtained hexagonal lattice assuming the same packing as the cubic one would produce a change in the number of molecules in the unit cell from 4 to 6, which matches with the experimental *Z* value obtained. It is worth mentioning that similar results were found for the cyclopentanol plastic phases.[54] In such a case, the two high temperature OD II and I phases were found to be hexagonal; the low temperature one had a *c*/*a* ratio of 0.94 (virtually the same value that in the present case, 0.97), whereas phase I was found to be close packed hexagonal, thus with the same packing as the FCC phase.

It should be noticed that the orientational disorder in phases I of both 2 Br A and 2 Cl A makes the overall packing indistinguishable from OD phases of 1 bromo (1 Br A) and 1 chlorine (1 Cl A) adamantane derivatives. In fact, the lattice parameter of 1 Br A was found to be 10.07 Å at 325 K, that is, 15 K above the transition from the low temperature ordered phase,[55] whereas for 2 Br A, it is found to be 10.00 Å at the same temperature from the phase transition from ordered phase II. Similar results can be evidenced when comparing 1 Cl A and 2 Cl A, 9.869[26] and 9.823 Å, both measured close to the phase transition to phase I. These experimental results evidence that substitution in tertiary or secondary carbons of halogen atoms gives rise to quite similar packing for adamantane derivatives as far as overall packing is concerned in the OD phases due to the primacy of the steric effects over the intermolecular interactions in the OD phases. Similar examples even involving molecular compounds displaying hydrogen bonding have previously been described to be governed by such geometric parameters.[56−59] At most, intermolecular interactions in OD phases play a crucial role into the dynamics of the reorientational molecular processes but have a really small effect on the packing of the OD structures.[33,60−62] Moreover, such reorientational processes, at least for the well known 1 X adamantane derivatives,are mainly dominated for the slower motions corresponding to the overall molecular tumbling, whereas the uniaxial rotations along the dipolar C_3 axis are much faster and with a much smaller activation energy.[30] Put in different words, these facts represent

the well known statement that translation and rotation have no effects on the experimental structure factors of the OD phases.[63] For 2 adamantanone, the only 2 X derivative studied so far by means of spectroscopic techniques, the same evidence has been reported.[34,64]

It should be mentioned that additional information can be reached from the diffraction patterns of disordered materials through the analysis of the structured diffuse scattering.[65,66] The analysis of the diffuse scattering together with the Bragg peaks (the total scattering) combined with Monte Carlo or molecular dynamics simulations can provide static and dynamic information that can far supersede spectroscopic methods.[67]

4.3. Thermodynamics. Table 1 gathers the thermodynamic values characterizing the phase transitions for both 2 Br A and 2 Cl A compounds determined in this work as well as the scarce set of values previously reported in the literature. It is worth mentioning that the small enthalpy value associated with the IV ($P1$) to III ($C2/c$) phase transition, an experimental fact that agrees with the small difference of the molecular packing and intermolecular interactions between both phases. On the same line of reasoning, identical arguments can be applied to the II (hexagonal) to I (FCC) phase transition for this compound (not reported in ref 39). Unfortunately, the low enthalpy changes of these transitions did not allow determining the two phase equilibrium lines in the corresponding $p-T$ phase diagram (Figure 2). As for 2 Br A compound, the experimental II–I pressure–temperature equilibrium line perfectly agrees with values reported by Hara et al.[38] obtained by means of density measurements as a function of pressure.

Lattice parameters as a function of temperature (Supporting Information) were measured from 90 to 370 K, and volume of the unit cells was thus calculated. Volume changes at the transitions were calculated by extrapolating the molar volumes at the transition temperatures, and they are compiled in Table 1. These values can be compared with those calculated by means of the Clausius–Clapeyron equation for the II–I of 2 Br A and IV–III of 2 Cl A phase transitions for which the pressure–temperature two phase equilibria were measured. It can be seen that values agree within the experimental error, providing a thermodynamic coherence of the reported values. Moreover, the robustness of the experimental values, at least as for 2 Br A, is highlighted when comparing the variation of the volume changes at the II–I phase transition as a function of pressure reported by Hara et al.[38] with the value at normal pressure determined in this work. (See the inset in Figure 10a.)

5. CONCLUSIONS

The polymorphism of 2 Br and 2 Cl adamantane derivatives has been studied from 90 K to the liquid state as well as a function of pressure (until 300 MPa). For 2 Br adamantane, the low temperature ordered phase, which has been found to be orthorhombic with space group $P2_12_12_1$ ($Z = 4$), transforms to the high temperature OD phase to which the space group $Fm3m$ has been assigned. No additional phase appears due to the increase in pressure within the studied range. As for 2 Cl adamantane, polymorphism is much richer, and four phases have been described. The lowest temperature phase IV has been characterized as triclinic ($P1$ space group, $Z = 2$). This phase transforms to a monoclinic ($C2/c$ space group, $Z = 8$) structure through a phase transition with small changes in both enthalpy and volume, thus confirming the similarity in packing and intermolecular interactions between both phases. The monoclinic phase transforms to an OD hexagonal phase (for which only Pawley refinement could be done) with $Z = 6$. Before melting, the hexagonal phase transforms to an OD $Fm3m$ phase with $Z = 4$, similar to that of 2 Br adamantane. Despite the $mm2$ molecular symmetry of the 2 X derivatives, the OD disorder makes compatible the molecular symmetry and the site lattice symmetry, as previously demonstrated for 2 adamantanone, the only 2 X adamantane derivative crystallographically described hitherto.[21]

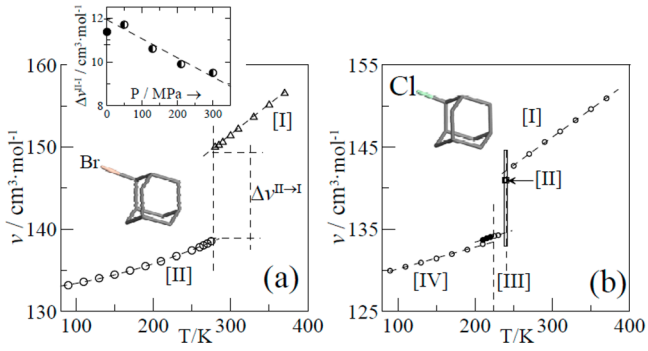

Figure 10. Molar volume of 2 Br A (a) and 2 Cl A (b) as a function of temperature derived from X ray diffraction experiments for the solid phases. Upper inset in panel a depicts the volume change for the II–I phase transition of 2 Br A as a function of pressure (half filled circles) from Hara et al.[38] and the corresponding value at normal pressure (filled circle) obtained in this work through X ray diffraction.

The molecular arrangement for all ordered phases here described shows that intermolecular interactions in 2 Br A are much weaker than those in 2 Cl A, a fact that has been found when building up interwoven complex diamondoid compounds in which Br atoms participate.[53] This study can thus help for the understanding of complex new adamantane based diamondoid complex structures as well as to rationalize those previously described with promising applications as building blocks of functional structures for nanotechnology.

AUTHOR INFORMATION

Corresponding Author

*Tel: +34 934016564. E mail: josep.lluis.tamarit@upc.edu.

Notes

The authors declare no competing financial interest.

ACKNOWLEDGMENTS

This work has been supported by the Spanish Ministry of Science and Innovation (grant FIS2008 00837) and the Catalan Government (grant 2014 SGR 581).

REFERENCES

(1) Elsaidi, S. K.; Mohamed, M. H.; Wojtas, L.; Chanthapally, A.; Pham, T.; Space, B.; Vittal, J. J.; Zaworotko, M. J. Putting the Squeeze on CH_4 and CO_2 through Control over Interpenetration in Diamondoid Nets. *J. Am. Chem. Soc.* **2014**, *136*, 5072–5077.

(2) Schoedel, A.; Zaworotko, M. $[M_3(\mu_3\ O)(O_2CR)_6]$ and Related Trigonal Prisms: Versatile Molecular Building Blocks for Crystal Engineering of Metal–Organic Material Platforms. *Chem. Sci.* **2014**, *5*, 1269–1282.

(3) Yamamoto, A.; Uehara, S.; Hamada, T.; Mivata, M.; Hisaki, I.; Tohnai, N. Diamondoid Porous Organic Salts toward Applicable Strategy for Construction of Versatile Porous Structures. *Cryst. Growth Des.* **2012**, *12*, 4600–4606.

(4) Gunawan, M. A.; Hierso, J. C.; Poinsot, D.; Fokin, A. A.; Fokina, N. A.; Tkachenko, B. A.; Schreiner, P. R. Diamondoids: Functionalization and Subsequent Applications of Perfectly Defined Molecular Cage Hydrocarbons. *New J. Chem.* **2014**, *38*, 28−41.
(5) Hohman, J. N.; Claridge, Sh. A; Kim, M.; Weiss, P. S. Cage Molecules for Self Assembly. *Mater. Sci. Eng., R* **2010**, *70*, 188−208.
(6) McIntosh, G. C.; Yoon, M.; Berber, S.; Tomanek, D. Diamond Fragments as Building Blocks of Functional Nanostructures. *Phys. Rev. B* **2004**, *70*, 045401.
(7) Wang, Y. Y.; Kiopakis, E.; Lu, X. H.; Wegner, D.; Yamachika, R.; Dahl, J. E.; Carlson, R. M. K.; Louie, S. G.; Crommie, M. F. Spatially Resolved Electronic and Vibronic Properties of Single Diamondoid Molecules. *Nat. Mater.* **2008**, *7*, 38−42.
(8) Yang, W. L.; Fabbri, J. D.; Willey, T. M.; Lee, J. R. I.; Dahl, J. E.; Carlson, R. M. K.; Schreiner, P. R.; Fokin, A. A.; Tkachenko, B. A.; Fokina, N. A.; et al. Monochromatic Electron Photoemission from Diamondoid Monolayers. *Science* **2007**, *316*, 1460−1462.
(9) Du, Q. S.; Huang, R. B. Recent Progress in Computational Approaches to Studying the M2 Proton Channel and Its Implication to Drug Design Against Influenza Viruses. *Curr. Protein Pept. Sci.* **2012**, *13*, 205−210.
(10) De Clercq, E. Antiviral Drugs in Current Clinical use. *J. Clin. Virol.* **2004**, *30*, 115−133.
(11) Nicholson, K. G.; Wood, J. M.; Zambon, M. Influenza. *Lancet* **2003**, *362*, 1733−1745.
(12) Cheon, Y. E.; Suh, M. P. Multifunctional Fourfold Interpenetrating Diamondoid Network: Gas Separation and Fabrication of Palladium Nanoparticles. *Chem.—Eur. J.* **2008**, *14*, 3961−3967.
(13) Espeau, P.; Céolin, R. Thermodynamics Studies of Solids with Non negligible Vapour Pressure: T v and p T Diagrams of the Dimorphism of Adamantane. *Thermochim. Acta* **2001**, *376*, 147−154 and references therein..
(14) Chang, S. S.; Westrum, E. F., Jr. Heat Capacities and Thermodynamic Properties of Globular Molecules. I. Adamantane and Hexamethylenetetramine. *J. Phys. Chem.* **1960**, *64*, 1547−1551.
(15) Nordman, C. E.; Schmitkons, D. L. Phase Transition and Crystal Structures of Adamantane. *Acta Crystallogr.* **1965**, *18*, 764−767.
(16) Wu, P. J.; Hsu, L.; Dows, D. A. Spectroscopy Study of the Phase Transition in Crystalline Adamantane. *J. Chem. Phys.* **1971**, *54*, 2714−2721.
(17) Amoureux, J. P.; Foulon, M. Comparison Between Structural Analyses of Plastic and Brittle Crystals. *Acta Crystallogr., Sect. B* **1987**, *43*, 470−479.
(18) Amoureux, J. P.; Bee, M.; Damien, J. C. Structure of Adamantane, $C_{10}H_{16}$, in the Disordered Phase. *Acta Crystallogr., Sect. B* **1980**, *36*, 2633−2636.
(19) Amoureux, J. P.; Bee, M.; Virlet, J. Anisotropic Molecular Reorientations of Adamantane in its Plastic Solid Phase: ^{1}H N.M.R. Relaxation Study in Solid Solutions of $C_{10}H_{16}$ and $C_{10}D_{16}$. *Mol. Phys.* **1980**, *41*, 313−324.
(20) Bee, M.; Amoureux, J. P.; Lechner, R. E. C_4 Rotational Jumps in Plastic Adamantane the Proof of their Existence and Uniqueness. *Mol. Phys.* **1980**, *40*, 617−641.
(21) Amoureux, J. P.; Bee, M. A Cubic Harmonic Analysis of the Plastic Crystal Structures of Adamantane, $C_{10}H_{16}$, and Adamantanone, $C_{10}H_{14}O$, at Room Temperature. *Acta Cryst. B* **1980**, *36*, 2636−2642.
(22) Arul Murugan, N.; Yashonath, S. Pressure Induced Ordering in Adamantane: A Monte Carlo Simulation Study. *J. Phys. Chem. B* **2005**, *109*, 2014−2020.
(23) Clark, Z.; Mcknox, O.; Mackle, H.; Mckervev, M. A. Order−Disorder Transitions in Substituted Adamantanes. *J. Chem. Soc., Faraday. Trans.* **1977**, *73*, 1224−1231.
(24) Virlet, J.; Quiroga, L.; Boucher, B.; Amoureux, J. P.; Castelain, M. Molecular Reorientations of 1 Bromo and 1 Iodo Adamantanes ^{1}H N.M.R. Relaxation Study. *Mol. Phys.* **1983**, *48*, 1289−1303.
(25) Braga, D.; Koetzle, T. F. Structure and Steric Hindrance Analyses to Determine the Dynamical Disorder in 1 Iodoadamantane ($C_{10}H_{15}I$). *Acta Crystallogr., Sect. B* **1988**, *44*, 156−163.
(26) Foulon, M.; Belgrand, T.; Gors, C.; More, M. Structural Phase Transition in 1 Chloroadamantane ($C_{10}H_{15}Cl$). *Acta Crystallogr., Sect. B* **1989**, *45*, 404−411.
(27) Affouard, F.; Hedoux, A.; Guinet, Y.; Denicourt, T.; Descamps, M. Indicationfor a Change of Dynamics in Plastic Crystal Chloroadamantane: Raman Scattering Experiment and Molecular Dynamics Simulation. *J. Phys.: Condens. Matter* **2001**, *13*, 7237−7248.
(28) Amoureux, J. P.; Sauvajol, J. L.; Bee, M. A Symmetry Adapted Function Analysis of Plastic Crystals. Application to 1 Cyanoadamantane at Room Temperature. *Acta Crystallogr., Sect. A* **1981**, *37*, 97−104.
(29) Amoureux, J. P.; Bee, M.; Sauvajol, J. L. Structure of 1 Fluoroadamantane, $C_{10}H_{15}F$, in its Plastic Phase. *Acta Crystallogr., Sect. B* **1982**, *38*, 1984−1989.
(30) Bee, M.; Amoureux, J. P. Molecular Reorientations of 1 Chloroadamantane in its Plastic Solid Phase. *Mol. Phys.* **1983**, *48*, 63−79.
(31) Betz, R.; Klüfers, P.; Mayer, P. 1 Bromoadamantane. *Acta Crystallogr., Sect. E* **2009**, *65*, o101.
(32) Bazyleva, A. B.; Blokhin, A. V.; Kabo, G. J.; Kabo, A. G.; Sevruk, V. M. Thermodynamic Properties of 2 Adamantanone in the Condensed and Ideal Gaseous States. *Thermochim. Acta* **2006**, *451*, 65−72.
(33) Romanini, M.; Negrier, P.; Tamarit, J. Ll.; Capaccioli, S.; Barrio, M.; Pardo, L. C.; Mondieig, D. Emergence of Glassy Like Dynamics in an Orientationally Ordered Phase. *Phys. Rev. B* **2012**, *85*, 134201.
(34) Brand, R.; Lunkenheimer, P.; Loidl, A. Relaxation Dynamics in Plastic Crystals. *J. Chem. Phys.* **2002**, *116*, 10386−10401.
(35) Hara, K.; Osugi, J. Pressure Induced Phase Transition in Adamantanone. *High Temp. High Pressures* **1980**, *12*, 221−223.
(36) Harvey, P. D.; Butler, I. S.; Gilson, D. F. R.; Wong, P. T. T. Raman Study of the Effect of High Pressure on the Order Disorder Phase Transition in 2 Adamantanone. *J. Phys. Chem.* **1986**, *90*, 4546−4549.
(37) Negrier, P.; Barrio, M.; Romanini, M.; Tamarit, J. Ll.; Mondieig, D.; Krivchikov, A. I.; Kepinski, L.; Jezowski, A.; Szewczyk, D. Polymorphism of 2 Adamantanone. *Cryst. Growth Des.* **2014**, *14*, 2626−2632.
(38) Hara, K.; Katou, Y.; Osugi, J. Pressure Induced Phase Transition and Compressive Behavior of Substituted Adamantanes. *Bull. Chem. Soc. Jpn.* **1981**, *54*, 687−691.
(39) Paroli, R. M.; Kawaii, A. T.; Butler, A. S.; Gilson, D. R. Phase Transitions in Adamantane Derivatives: 2 Chloroadamantane. *Can. J. Chem.* **1988**, *66*, 1973−1978.
(40) Hara, K.; Taniguchi, J.; Suzuki, K. Pressure Induced Phase Transition in 2 Methyladamantane and 2 Bromoadamantane. *Chem. Lett.* **1980**, 803−806.
(41) Charapennikau, M. B.; Blokhin, A. V.; Kabo, A. G.; Kabo, G. J. The Heat Capacities and Parameters of Solid Phase Transitions and Fusion for 1 and 2 Adamantanols. *J. Chem. Thermodyn.* **2003**, *35*, 145−157.
(42) Salman, S. R.; Harris, R. K.; Lindon, J. C. An Investigation of Solid State Phase Transitions in 1 Adamantanol and 2 Adamantanol by C 13 CP MAS NMR. *Thermochim. Acta* **1991**, *179*, 295−300.
(43) Lutz, B. T. G.; van der Maas, J. H. The Sensorial Potentials of the OH Stretching Mode. *J. Mol. Struct.* **1997**, *436−437*, 213−231.
(44) Würflinger, A. Differential Thermal Analysis Under High Pressure IV: Low Temperature DTA of Solid Solid and Solid Liquid Transitions of Several Hydrocarbons up to 3 kbar. *Ber. Bunsen. Phys. Chem.* **1975**, *79*, 1195−1201.
(45) Reuter, J.; Büsing, D.; Tamarit, J. Ll.; Würflinger, A. High Pressure Differential Thermal Analysis Study of the Phase Behaviour in Some tert Butyl Compounds: Pivalic Acid, 2 Methylpropane 2 thiol and tert Butylamine. *J. Mater. Chem.* **1997**, *7*, 41−46.

(46) Ballon, J.; Comparat, V.; Pouxe, J. The Blade Chamber: A Solution for Curved Gaseous Detectors. *Nucl. Instrum. Methods* **1983**, *217*, 213−216.
(47) Evain, M.; Deniard, P.; Jouanneaux, A.; Brec, R. Potential of the INEL X ray Position Sensitive Detector: a General Study of the Debye Scherrer Setting. *J. Appl. Crystallogr.* **1993**, *26*, 563−569.
(48) *MS Modeling (Materials Studio)*, version 5.5. http://www.accelrys.com.
(49) Toraya, H.; Marumo, F. Preferred Orientation Correction in Powder Fitting. *Mineral. J.* **1981**, *10*, 211−221.
(50) Rietveld, H. M. A Profile Refinement Method for Nuclear and Magnetic Structures. *J. Appl. Crystallogr.* **1969**, *2*, 65−71.
(51) Shimoikeda, Y.; Machida, M. ^{1}H NMR Study of Phase Transition in 2 Bromoadamantane. *J. Korean Phys. Soc.* **1999**, *35*, S1423−S1425.
(52) Pawley, G. S.; Whitley, E. Structure of Sym $C_2F_4Br_2$. *Acta Cryst., Sect. C* **1988**, *44*, 1249−1251.
(53) Guo, W.; Galoppini, E.; Gilardi, R.; Rydja, G. I.; Chen, Y. H. Weak Intermolecular Interactions in the Crystal Structures of Molecules with Tetrahedral Symmetry: Diamondoid Nets and Other Motifs. *Cryst. Growth Des.* **2001**, *1*, 231−237.
(54) Rute, M. A.; Salud, J.; López, D. O.; Tamarit, J. Ll.; Negrier, P.; Barrio, M.; Mondieig, D. Polymorphism of Cyclopentanol: Crystallographic Characterization of the Ordered and Disordered Phases. *Chem. Mater.* **2003**, *15*, 4725−4731.
(55) Bazyleva, A. B.; Blokhin, A. V.; Kabo, G. J.; Kabo, A. G.; Paulechka, Y. U. Thermodynamic Properties of 1 Bromoadamantane in the Condensed State and Molecular Disorder in its Crystals. *J. Chem. Thermodyn.* **2005**, *37*, 643−657.
(56) Barrio, M.; López, D. O.; Tamarit, J. Ll.; Negrier, P.; Haget, Y. Molecular Interactions and Packing in Molecular Alloys Between Non Isomorphous Plastic Phases. *J. Solid State Chem.* **1996**, *124*, 29−38.
(57) Salud, J.; Barrio, M.; López, D. O.; Alcobé, X.; Tamarit, J. Ll. Anisotropy of the Intermolecular Interactions from the Study of the Thermal Expansion Tensor. *J. Appl. Crystallogr.* **1998**, *31*, 748−757.
(58) Salud, J.; López, D. O.; Barrio, M.; Tamarit, J. Ll.; Oonk, H. A. J.; Haget, Y.; Negrier, Ph. On the Crystallography and Thermodynamics in Orientationally Disordered Phases. *J. Solid State Chem.* **1997**, *133*, 536−544.
(59) Salud, J.; López, D. O.; Barrio, M.; Tamarit, J. Ll. Two Component Systems of Isomorphous Orientationally Disordered Crystals. Part I: Packing of the Mixed Crystals. *J. Mater.Chem.* **1999**, *9*, 909−916.
(60) Tamarit, J. Ll.; Perez Jubindo, M. A.; de la Fuente, M. R. Dielectric Studies on Orientationally Disordered Phases of Neopentylglycol ($(CH_3)_2C(CH_2OH)_2$) and Tris(hydroxymethyl) aminomethane ($NH_2C(CH_2OH)_3$). *J. Phys.: Condens. Matter* **1997**, *9*, 5469−5478.
(61) Pothoczki, Sz.; Ottochian, A.; Rovira Esteva, M.; Pardo, L. C.; Tamarit, J. Ll.; Cuello, G. J. Role of Steric an Electrostatic Effects in the Short Range Order of Quasi Tetrahedral Molecular Liquids. *Phys. Rev. B* **2012**, *85*, 014202.
(62) Pardo, L. C.; Tamarit, J. Ll.; Veglio, N.; Bermejo, F. J.; Cuello, G. J. Comparison of Short Range Order in Liquid and Rotator Phase States of a Simple Molecular Liquid: a Reverse Monte Carlo and Molecular Dynamics Analysis of Neutron Diffraction Data. *Phys. Rev. B* **2007**, *76*, 134203.
(63) Press, W.; Grimm, H.; Holler, A. Analysis of Orientationally Disordered Structures. IV. Correlations Between Orientation and Position of a Molecule. *Acta Cryst., Sect. A* **1979**, *35*, 881−885.
(64) Bee, M.; Amoureux, J. P. Quasielastic Neutron Scattering Study of Reorientational Motions in 2 Adamantanone $C_{10}H_{14}O$. *Mol. Phys.* **1982**, *47*, 533−550.
(65) Coulon, G.; Descamps, M. Neutron Diffuse Scattering in the Disordered Phase of CBr_4. II. Theoretical Evidence of Steric Hindrance. *J. Phys. C: Solid State Phys.* **1980**, *13*, 2847−2856.
(66) Descamps, M.; Caucheteux, C.; Odou, G.; Sauvajol, J. L. Local Molecular Order in the Glassy Crystalline Phase of Cyanoadamantane: Diffuse X ray Scattering Analysis. *J. Phys., Lett.* **1984**, *45*, 719−727.
(67) Thomas, L. H.; Welberry, T. R.; Goossens, D. J.; Heerdegen, A. P.; Gutmann, M. J.; Teat, S. J.; Lee, P. L.; Wilson, C. C.; Cole, J. M. Disorder in Pentachloro nitrobenzene, $C_6Cl_5NO_2$: A Diffuse Scattering Study. *Acta Cryst., Sect. B* **2007**, *63*, 663−673.